Oxidative Degradation of Trichloroethylene over Fe₂O₃-doped Mayenite: Chlorine Poisoning Mitigation and Improved Catalytic Performance

Raffaele Cucciniello [1,†] ⓘ, **Adriano Intiso** [1,†], **Tiziana Siciliano** [2], **Antonio Eduardo Palomares** [3,*] ⓘ, **Joaquín Martínez-Triguero** [3] ⓘ, **Jose Luis Cerrillo** [3] ⓘ, **Antonio Proto** [1] and **Federico Rossi** [4,*] ⓘ

1   Department of Chemistry and Biology, University of Salerno, via Giovanni Paolo II, 132, 84084 Fisciano (SA), Italy
2   DiSTeBa Department, University of Salento, 73100 Lecce (LE), Italy
3   Instituto de Tecnología Química, Universitat Politècnica de València-CSIC, Valencia 46022, Spain
4   Department of Earth, Environmental and Physical Sciences, DEEP Sciences, Pian dei Mantellini 44, 53100 Siena, Italy
*   Correspondence: apalomar@iqn.upv.es (A.E.P.); federico.rossi2@unisi.it (F.R.)
†   These authors contributed equally to this work.

Abstract: Mayenite was recently successfully employed as an active catalyst for trichloroethylene (TCE) oxidation. It was effective in promoting the conversion of TCE in less harmful products (CO₂ and HCl) with high activity and selectivity. However, there is a potential limitation to the use of mayenite in the industrial degradation of chlorinated compounds—its limited operating lifespan owing to chlorine poisoning of the catalyst. To overcome this problem, in this work, mayenite-based catalysts loaded with iron (Fe/mayenite) were prepared and tested for TCE oxidation in a gaseous phase. The catalysts were characterized using different physico-chemical techniques, including XRD, ICP, N₂-sorption (BET), H₂-TPR analysis, SEM-EDX, XPS FESEM-EDS, and Raman. Fe/mayenite was found to be more active and stable than the pure material for TCE oxidation, maintaining the same selectivity. This result was interpreted as the synergistic effect of the metal and the oxo-anionic species present in the mayenite framework, thus promoting TCE oxidation, while avoiding catalyst deactivation.

Keywords: trichloroethylene; mayenite; catalytic oxidation; iron; chlorine poisoning

1. Introduction

Trichloroethylene (TCE) is a chlorinated volatile organic solvent belonging to the class of dense non aqueous phase liquids (DNAPL) pollutants [1–3]. Several strategies have been considered for TCE remediation, including the use of CaO [4], bioremediation [5,6] and adsorption processes with activated charcoal or zeolites [7,8]. In addition, as TCE is highly volatile, it can be easily stripped from the remediation media (water, surfactant solutions, removed soils, etc.) with air flux and directed to further treatments in gas phase [9,10]. In this respect, catalytic heterogeneous oxidation is becoming a popular alternative to thermal incineration for treating exhausted gases rich in TCE, as catalysts lower operative temperatures and improve selectivity of the reaction towards less harmful products, with high benefits in terms of energy consumption and environmental impact.

Several heterogeneous catalysts have been developed and tested for gaseous TCE oxidation. Catalytic systems based on noble metals, particularly Pt and Pd, have been extensively employed, showing good results in terms of activity and selectivity, as reported by Gonzalez-Velasco and co-workers in a recently published review [11]. Less-expensive catalysts, based on metallic oxides, have

also been prepared as uniform catalyst or supported on high surface materials (e.g., γ-Al_2O_3) [12,13]. Blanch-Raga et al. reported the oxidation of TCE over different mixed oxides derived from hydrotalcites [14], with the Co(Fe/Al) catalyst being the most active ($T_{50\%}$ = 280 °C and $T_{90\%}$ = 340 °C at Gas Hourly Space Velocity, GHSV = 15,000 h^{-1} and [TCE] = 1000 ppm) due to its acidic and oxidative properties. Zeolites also represent an important type of active catalysts for the oxidation of TCE and many papers have reported on the synergic effect of acidic sites in zeolites [15] with metal catalysts in order to improve the performance of the whole catalytic system. Romero-Saez et al. [16], studied the performance of iron-doped ZSM-5 zeolite for TCE oxidation, finding that a ZSM-5 containing 2 wt% of Fe quantitatively oxidizes 1000 ppm of TCE at 500 °C and GHSV = 13,500 h^{-1}. This paper shows that the formation of active iron (III) species, as Fe_2O_3 nanoparticles, was most likely responsible for the enhanced catalytic performance of the zeolite. Nevertheless the catalyst suffers some deactivation after 16 h of reaction due to the formation of $FeCl_3$ [16]. Recently, Palomares et al. reported a remarkably high selectivity towards CO_2 during TCE oxidation with Cu and Co-doped beta zeolites. The best results ($T_{50\%}$ = 310 °C and $T_{90\%}$ = 360 °C at GHSV = 15,000 h^{-1} and [TCE] = 1000 ppm) were obtained by using Cu-doped zeolite, which combined the acid sites of the zeolite with the redox properties of the copper ions [17]. Notwithstanding, zeolites-based catalysts suffer some drawbacks, which include coke formation, deactivation, and formation of chlorinated by-products [14].

In previous works, we reported about the oxidation of TCE by using the mesoporous calcium aluminate mayenite ($Ca_{12}Al_{14}O_{33}$) as a catalyst [18–22]; mayenite had a good overall performance, showing high activity and selectivity towards nontoxic compounds, and fair thermal stability and recyclability. As a main drawback, the material shows a certain tendency towards chlorine poisoning, leading to slow deactivation of the catalyst. Mayenite has a zeolite-type structure with interconnected cages and a positive electric charge per unit cell that is balanced by O^{2-} ions (free oxygen ions) [23]. The free oxygen ions can be substituted by other species (Cl^-, H^-, NH_2^-, etc.) [24,25] and can migrate from the bulk to the surface at temperatures higher than 400 °C [26], thus conferring to the mayenite oxidative properties exploited for many applications [27–29]; for instance, as Ni support for the catalytic reforming of tar [30–32].

With the aim of further improving mayenite activity for TCE oxidation and mitigating deactivation of the material, in this work, we use a mayenite containing iron that is employed for the catalytic oxidation of TCE. The performance of the system has been evaluated by means of the light-off curve and the structural properties of the material have been characterized, before and after the reaction, by means of different physico-chemical techniques, including XRD, ICP analysis, N_2-sorption (BET), H_2-TPR analysis, SEM-EDX, FESEM-EDS, XPS, and Raman spectroscopy. We have prepared catalysts with different iron content and compared the activity and stability of this material with those of pure mayenite.

2. Results and Discussion

Figure 1 shows the XRD patterns of mayenite and Fe/Mayenite loaded with 2% of Fe_2O_3 (1.5% Fe/mayenite has an identical spectrum). The mayenite XRD pattern presented typical peaks of mayenite around 2θ = 18.1°, 30°, 33.4°, 36.7°, 41.2°, 46.7°, 55.2° and 57.4°. $Ca_3Al_2O_6$ (●) and $CaAl_2O_4$ (Δ) were also found as impurities formed during the mayenite preparation processes [33].
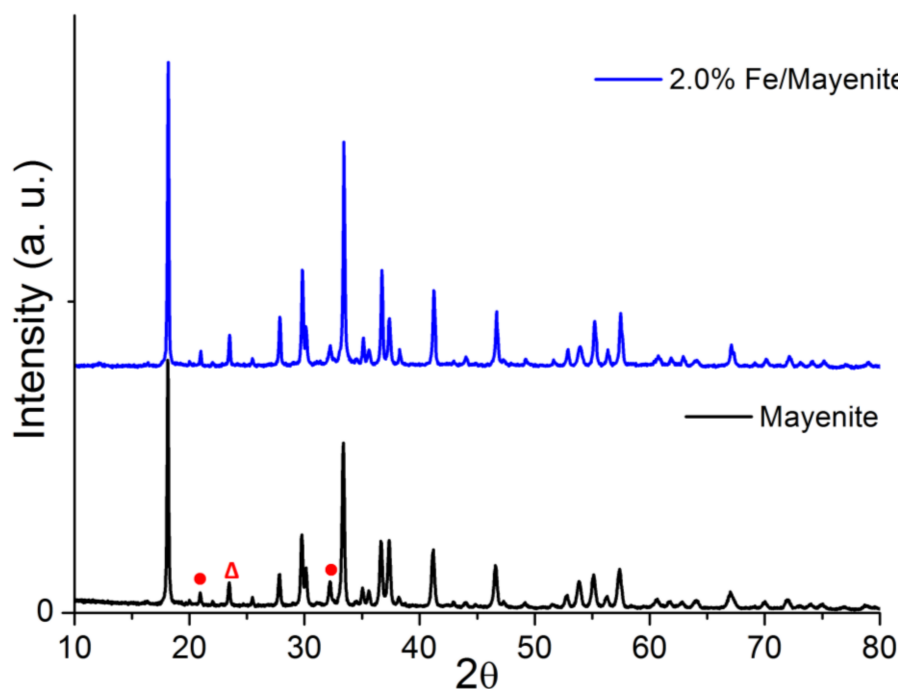
Figure 1. XRD patterns of mayenite (black) and 2.0% Fe/mayenite (blue).

The Fe/mayenite catalyst clearly maintains the crystalline structure of mayenite. Furthermore, no peaks associated with iron oxides were observed in the Fe/mayenite samples; this is due to the low metal loading in the mayenite and their good dispersion on the mayenite support [34].

Table 1 shows the metal loading and specific surface area of the catalysts. The BET surface area of mayenite was 11.7 m^2/g, in line with data reported for this type of material [27]. The Fe/mayenite samples had BET surface area values similar to that of mayenite, showing that the incorporation of iron does not modify its textural properties. ICP analysis confirmed that the iron content was close to the nominal value.

Table 1. Iron content and BET surface area of the catalysts.

Catalyst	Fe Content (wt.%)	BET Surface Area (m^2/g)
Mayenite	-	11.7
1.5% Fe/mayenite	1.72	11.5
2.0% Fe/mayenite	2.30	11.2

Fe/mayenite is a porous material (view SI, Figure S1), characterized by large pores with dimensions of μm (macropores) and nm (mesopores) composed of calcium, aluminium, oxygen, and iron with an approximate content of 34%, 40%, 26%, and 2 wt.%, respectively. The structure and composition of the synthetized materials were also characterised by FESEM-EDS analysis, which yielded similar results, but allowed a detailed distribution of the atomic content. Figure 2 shows the results obtained, observing the most abundant elements in mayenite, i.e., aluminium, calcium, and oxygen. Iron atoms appear in low quantity and with a homogenous distribution in the mayenite, demonstrating good iron dispersion on the mayenite support. Moreover, the FESEM images of Fe/mayenite and pure mayenite (not shown) showed no significant differences in terms of morphology, maintaining the typical morphology of mayenite in both cases.
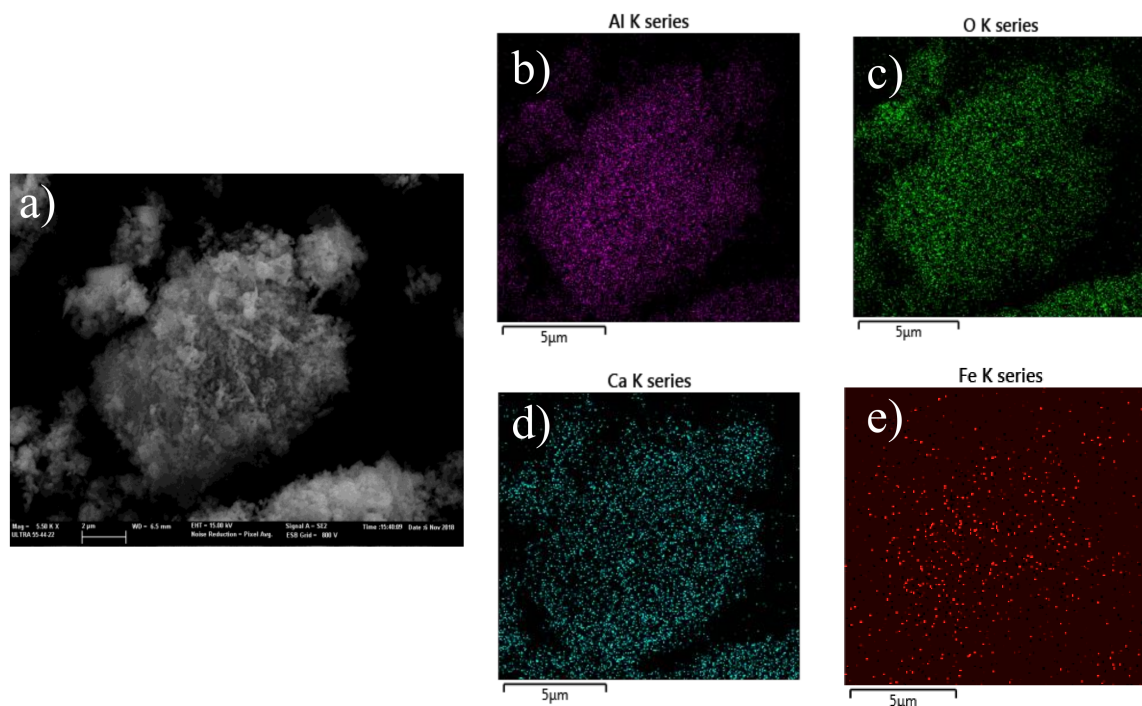
Figure 2. (**a**) FESEM micrograph (magnification of × 5500) of Fe/mayenite; atomic mapping of Fe/mayenite: (**b**) Al (purple); (**c**) O (green); (**d**) Ca (blue); (**e**) Fe (red).

TPR study of the catalysts is reported in Figure 3. All samples have similar hydrogen consumption, but present different TPR profiles. As can be seen, two peaks are observed for mayenite: the first one is a smaller band that appears around 550 °C, while the second is more intense and has the maximum at 620 °C. The first corresponds to the dissociative adsorption of H_2 in a heterolitic fashion [35] and the second to the reaction of these species with extra framework O_x^- and O_2^{2-} anions [36]. Iron-containing mayenites show a different profile with a unique band centred at 550 °C for the sample with 1.5% Fe or at 530 °C for the sample containing 2% Fe. These bands are assigned to the reduction of extra framework O_x^- and O_2^{2-} anions that in these catalysts are coincident with the band assigned to the dissociative adsorption of H_2 with consequential water formation, as previously reported for iron oxide-based catalysts [37]. Also, a small shoulder at 400–450 °C can be observed in the sample with higher iron content. This shoulder is assigned to the reduction of Fe^{3+} to Fe^{2+}, as reported by Romero-Saez et al. for Fe/zeolite samples [16]. Quantification of the hydrogen consumption shows similar results for the different samples, as the main species reduced in all the catalysts are the anionic oxygens present in the mayenite. The low iron content of the Fe/mayenite and the only partial reaction of the Fe^{3+} species results in a negligible consumption of hydrogen compared to that necessary for the oxygen species reduction. The results also show that there is a relationship between the content of iron and the shift towards lower temperatures of the extra framework O_x^- and O_2^{2-} reduction peak. This indicates that there is an interaction between iron species and anionic oxygen, which improves the redox properties of the catalysts containing iron.
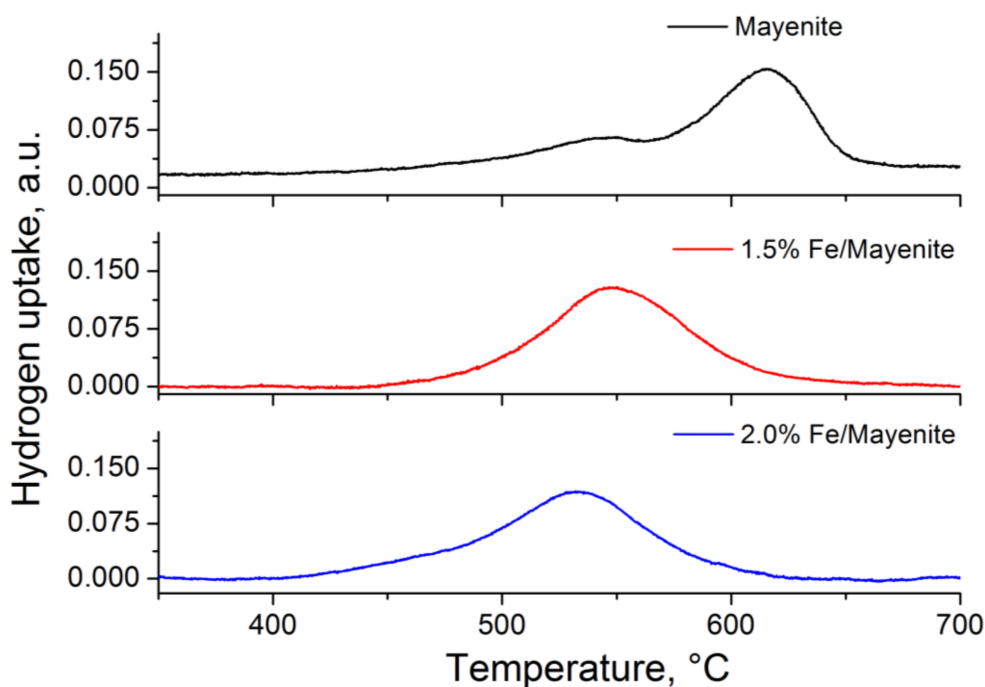
Figure 3. H_2-TPR profiles of mayenite (black), 1.5% Fe/mayenite (red), and 2.0% Fe/mayenite (blue).

The synthetized catalysts have been evaluated for oxidation of trichloroethylene by monitoring the conversion percentage calculated by means of Equation (1) as a function of the temperature (light-off curve). As shown in Figure 4, 2.0% Fe/mayenite has the best conversion rate among the different catalysts tested.
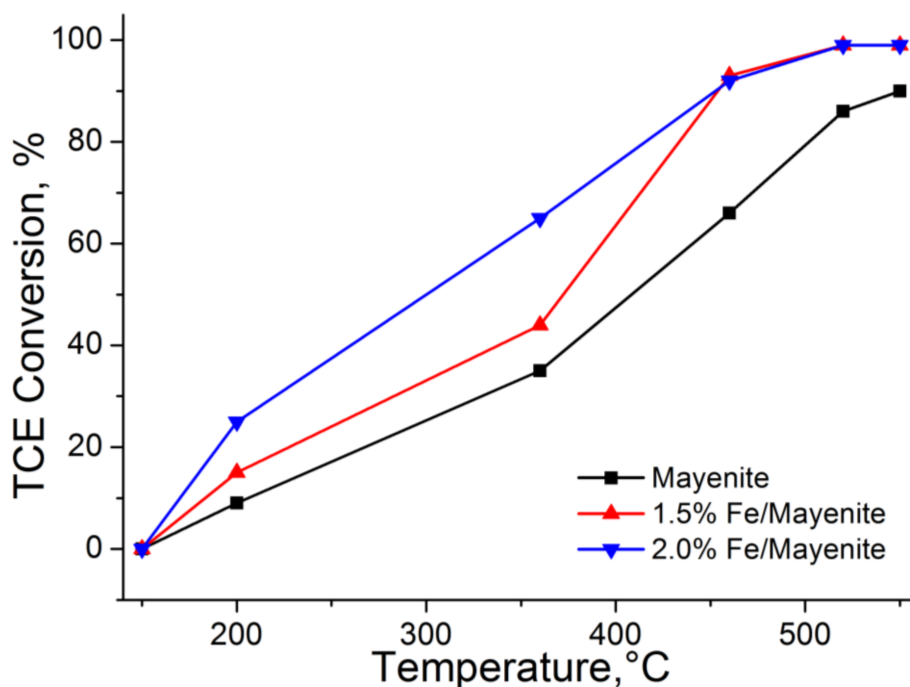

Figure 4. TCE conversion in wet conditions for mayenite (black), 1.5% (red), and 2.0% (blue) Fe/mayenite.

Blank experiments performed without a catalyst showed no significant TCE conversion below 550 °C. T_{50} and T_{90} (temperature at which 50% and 90% of the TCE was depleted, respectively) were found significantly lower for Fe/mayenite, with respect to pure mayenite (Table 2). In particular,

pure mayenite, used as a reference, showed T_{50} = 410 °C and T_{90} = 550 °C; 2.0% Fe/mayenite has a T_{50} = 300 °C and T_{90} = 460 °C and for 1.5% Fe/mayenite T_{50} was found slightly higher (375 °C), whilst T_{90} was the same as 2.0% iron-loaded mayenite. Conversion rates at 365 °C were also calculated according to Equation (2) for the three catalysts and reported in Table 2. Preliminary experiments revealed that an iron loading higher than ~2% in the mayenite did not significantly improve the conversion performance.

Table 2. Catalysts activity in terms of T_{50} and T_{90} and conversion rate at 365 °C.

Catalyst	T_{50} (°C)	T_{90} (°C)	Conversion Rate (mol g^{-1} s^{-1})
Mayenite	410	550	5.58×10^{-6}
1.5% Fe/mayenite	375	460	7.14×10^{-6}
2.0% Fe/mayenite	300	460	1.05×10^{-5}

The results show an increased catalytic activity of mayenite in the presence of iron. This can be explained by the synergistic effect of dispersed iron with the ionic oxygen species (O^{2-} and O_2^{2-}) present in the mayenite framework. In fact, iron species have a twofold role: *i*) they are active oxidants [11,16] and, *ii*) they make easier the interaction of the atmospheric O_2 to form O^{2-} and O_2^{2-}, responsible for the TCE oxidation [26]. Both roles result in improved redox and catalytic properties for Fe/mayenite, when compared with pure mayenite, as the TPR and catalytic results have shown.

The results of selectivity tests showed that, for all the catalysts, CO_2 and CO were the main oxidation reaction products (CO/CO_2 ratio was 50:50 for all the investigated temperatures and catalysts), while only HCl was detected as a chlorinated product.

2% Fe/mayenite stability was evaluated for several hours (12 h) at stationary conditions (T = 460 °C, 1700 ppm TCE, GHSV = 6000 h^{-1}, 0.8 g of catalyst). As highlighted in Figure 5, the presence of iron on the mayenite surface drastically improved the stability of the material. Indeed, after 2 h of reaction, pure mayenite showed a significant loss in activity, whilst 2.0% Fe/mayenite retained catalytic activity. Only a partial deactivation of the 2% Fe/mayenite catalyst was observed after 12 h of reaction, decreasing the conversion from 95% to 80%.
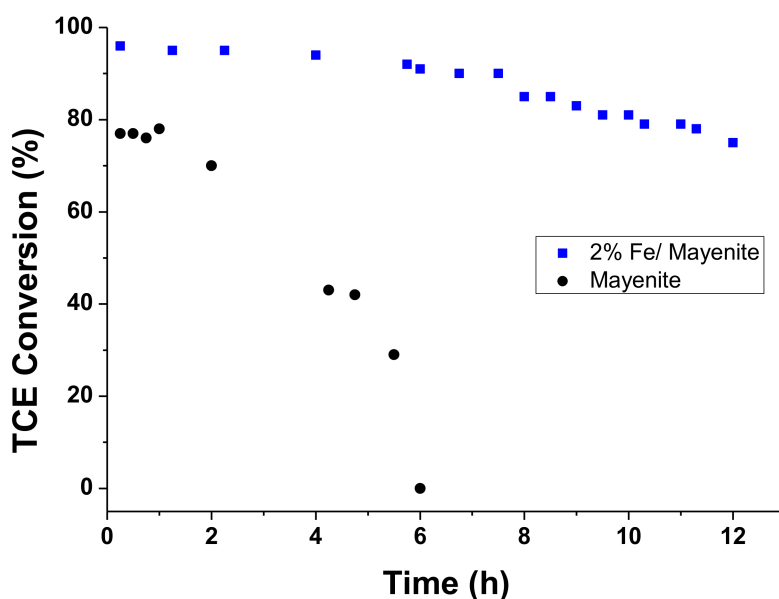

Figure 5. Comparison of catalyst stability (T = 460 °C, 1700 ppm TCE, GHSV = 6000 h^{-1}, 0.8 g of catalyst).

These results are interesting because stability of the catalyst is essential for possible commercial use of the material. As reported in previous works, the deactivation mechanism of mayenite catalyst is related with the displacement of active oxygen species by chloride ions [19,20,24,25]. In particular, the formation of HCl during the reaction caused a partial irreversible substitution of the anionic oxygen species ($O_x{}^{x-}$) by chloride ions forming chloromayenite [19,22], with consequent deactivation of the catalyst. It is observed that the presence of iron in mayenite modifies this mechanism, probably because the Fe species catalyze the interaction of the atmospheric O_2 to form O^{2-} and $O_2{}^{2-}$, making reversible the substitution of chloride ions by oxygen and avoiding or diminishing the formation of chloromayenite. In order to understand the role of iron in improving the stability of the material, XRD, SEM-EDX, FESEM-mapping, XPS, and Raman analyses of fresh and used catalysts were performed. XRD patterns and SEM images did not show important differences before and after the reaction, indicating a high structural stability of the material both in the absence and in the presence of iron (see Supplementary Materials for details, Figures S2 and S3a). Nevertheless, the EDX spectrum (Figure S3b) of the 2% Fe/mayenite sample after the stability test shows the presence of chloride. This is clearly observed in Figure 6 with the atomic mapping of Fe/mayenite after reaction. Comparing these images with those of the catalyst before reaction (Figure 2), it is observed that after the 12 h reaction, mayenite has the same morphology and distribution as Ca, Al, O and Fe atoms, revealing high stability of Fe/mayenite. It is observed that iron atoms do not agglomerate after reaction, indicating high stability of the metal supported on the mayenite. The main difference with the material before reaction is the presence of Cl atoms (orange points). The Cl mapping shows that this element has the same distribution as Ca atoms, suggesting that Cl is mainly interacting with Ca, because the basic properties of this element favour interaction with an acidic molecule as HCl. Different distribution of Cl and Fe atoms suggests that $FeCl_3$ was not formed, as it occurs in zeolites [16], indicating a high stability of the Fe species not poisoned by the chloride present on the catalyst surface.
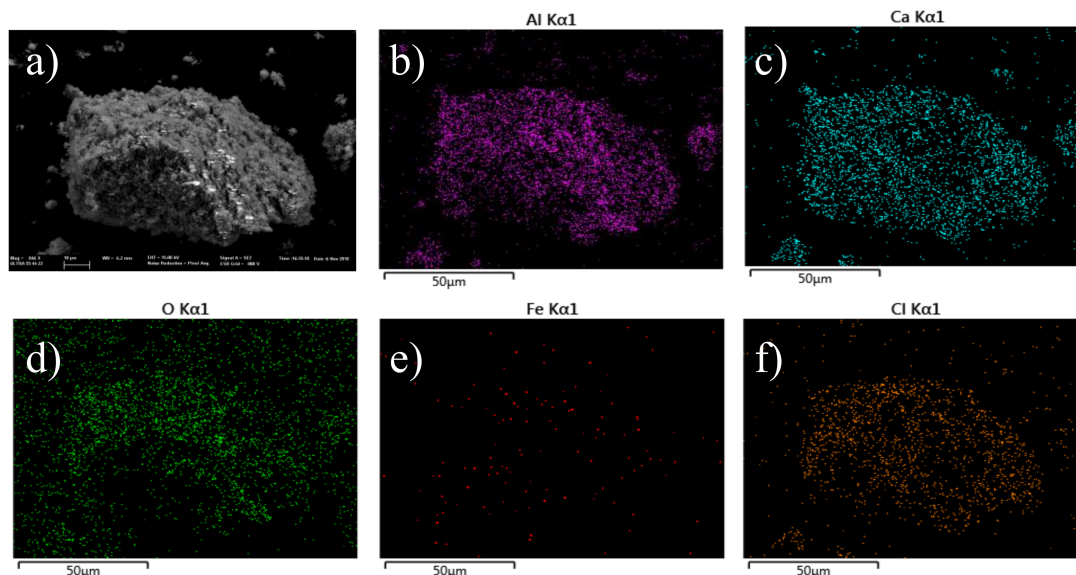

Figure 6. (**a**) FESEM micrograph (magnification of × 5500) of post-reaction Fe/mayenite; atomic mapping of post-reaction Fe/mayenite: (**b**) Al (purple); (**c**) O (green); (**d**) Ca (blue); (**e**) Fe (red); (**f**) Cl (orange).

The full XPS spectra of the mayenite containing iron before and after reaction are shown in Fig S4, where a peak at 200 eV is observed in the sample after reaction corresponding to the binding energy of Cl (2p) with two contributions at 200 and 189.7 eV, characteristic of Cl ($2p_{3/2}$) and Cl ($2p_{1/2}$ for ionic chlorine (Cl^-) [38]. The presence of this peak in the sample after reaction coincides with a decrease in the relative intensity of the O peak at 530.9 eV due to the oxygen surface species consumption during the reaction. On the other hand, Figure 7 shows a complex multiplet-split Fe 2p XPS spectra.

At least two contributions are observed: the first one is centred at 709.5 eV and the second, which is more intense, is centred at 711.8 eV. These peaks have been assigned to Fe^{2+} ($2p_{3/2}$) and Fe^{3+} ($2p_{3/2}$), respectively, indicating the formation of Fe_2O_3, probably together with Fe_3O_4 [38,39]. After reaction, an increase in the band centred at 711.8 eV, together with a small shift to the highest eV, is observed; it could be related with the disappearance of the Fe^{2+} contribution in the Fe_3O_4 phase or the formation of $FeCl_3$ [39]. These results reveal that after 12 h of reaction, part of the HCl formed in the reaction interacts with the mayenite and some chloride species are formed on the catalyst surface. Nevertheless, these species are not irreversibly adsorbed on the ionic vacancies (as in the case with pure mayenite [19,22]) and oxidant centres (anionic oxygen) are present after reaction. This is due to a synergic action of the iron present in the mayenite surface, which catalyses O_x^{x-} regeneration with the gas-phase oxygen present in the reaction media.
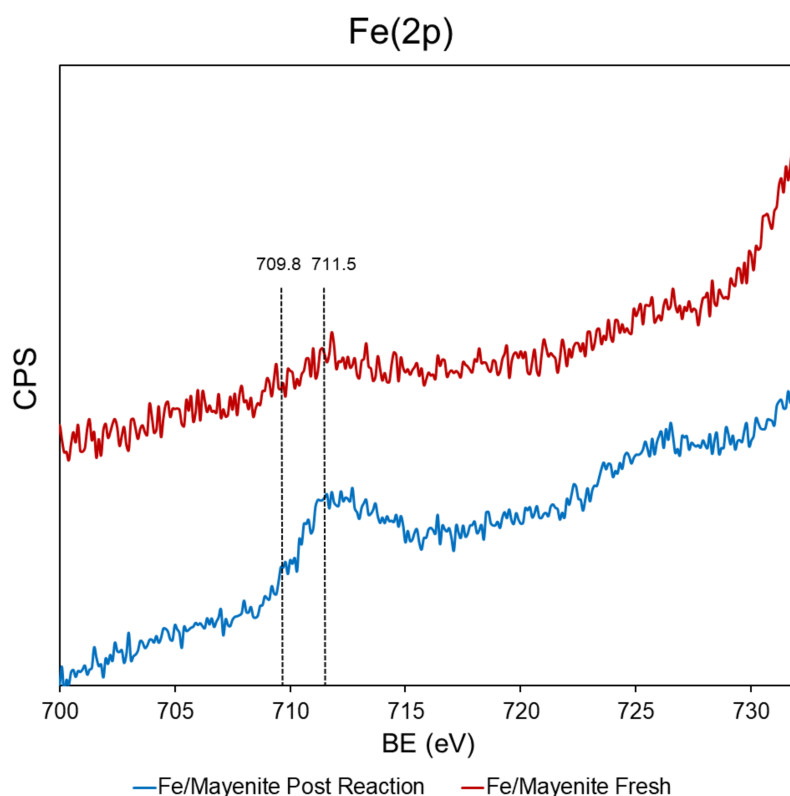

Figure 7. XPS spectra for the Fe (2p) of the Fe/mayenite (2% Fe) before and after reaction.

To understand this process better, Raman spectroscopy studies were conducted; the results are given in Figure 8. It is shown that in Fe/mayenite, the signal for oxygen O_2^- at 1075 cm^{-1} is preserved after the catalytic test. Similar results were obtained in the XPS analysis of the samples after reaction (see Supplementary Materials). This does not occur with pure mayenite [19,22], demonstrating that the redox properties of iron catalyze the regeneration of anionic oxygen by the O_2 present in the gas feed and avoid the irreversible chlorine poisoning of mayenite.
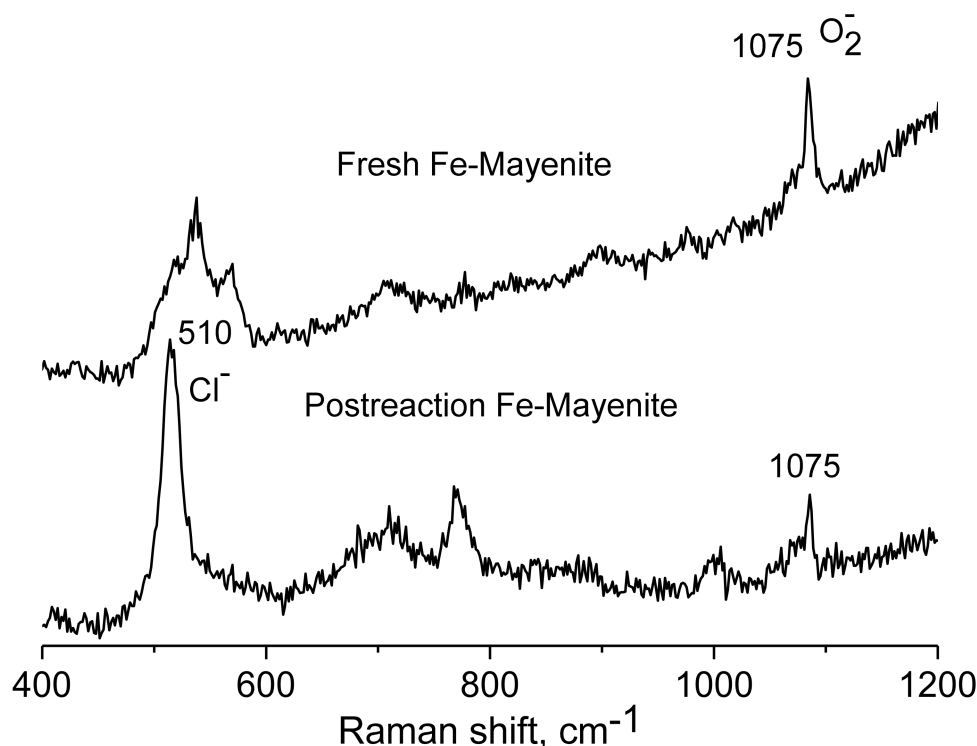
Figure 8. Raman spectra of Fe/mayenite (2.0%), fresh (top) and after reaction (bottom).

These results clearly show that the presence of well-dispersed iron on the mayenite surface improves the redox properties of the mayenite together with its stability, due to the ability of iron to catalyse the regeneration of the anionic oxygen responsible for TCE oxidation.

3. Materials and Methods

3.1. Materials

Trichloroethylene, calcium hydroxide, aluminium hydroxide, iron (III) acetylacetonate ($Fe(acac)_3$), toluene, and nitric acid were purchased from Sigma Aldrich and used without further purification.

3.2. Catalyst Preparation and Characterization

Details on the experimental methods are reported in the Supplementary Materials; here, we briefly sketch the basic procedures employed in this work. Mayenite was prepared by following the ceramic method described by Li et al. [40], starting with a mixture of calcium and aluminium hydroxide. Successively, mayenite was loaded with two different amounts of iron (1.5 and 2.0%) by using a solution of $Fe(acac)_3$ [41].

Diffraction patterns were recorded on a Bruker D8 Advance automatic diffractometer, operating with nickel-filtered CuKα radiation.

The iron content of Fe/mayenite catalyst was determined by ICP-OES analysis using a Perkin Elmer Optima 7000 DV after digestion of the sample in HNO_3. Three replicates for each sample were made.

The BET surface areas were determined with an 11-point BET analysis, after a degassing procedure in vacuum at 200 °C, by using a Nova Quantachrome 4200e instrument.

Temperature programmed reduction (TPR) of samples (10–20 mg) was measured with a TPD-TPR Autochem 2910 analyzer in the range of 25–800 °C.

The morphological and elemental analysis of the catalysts was performed by a scanning electron microscope (SEM, Tescan Vega LMU) equipped with a X-Ray energy dispersive microanalysis of

elements (EDX, Bruker Quantax 800). Additionally, Fe/mayenite was characterized by field emission scanning electronic microscope (FESEM, ZEISS ULTRA 55).

X-ray photoelectron spectroscopy (XPS) was performed by using a SPECS spectrometer equipped with a Phoibos 150MCD-9 multichannel analyser. CasaXPS software was used for spectra treatment.

Raman spectra were recorded at RT with a 514 nm laser excitation on a Renishaw Raman Spectrometer (in via) equipped with a CCD detector. The laser power on the sample was 25 mW and a total of 20 acquisitions were taken for each spectra.

3.3. Experimental Setup and Catalytic Reactions

The experiments were performed in a stainless-steel fixed bed reactor, with the catalysts (0.8 g) placed between two quartz fiberglass stoppers. The cylindrical reactor (150 mm × 18 mm i.d., 22 mm o.d.) was placed in a furnace and the temperature was controlled via a K-thermocouple located inside the reactor.

Catalytic oxidations were monitored in the temperature range of 150–550 °C and the catalysts were kept at an operative temperature in air for 30 min before flow of TCE. The inlet gas was prepared by flowing a stream of air through pure TCE at room temperature; the final gas composition was [TCE] = 1700 ppm in wet air (RH = 60%). The Gas Hourly Space Velocity (GHSV) was set to 6000 h^{-1} by flowing the inlet gas at 110 mL/min. The residence time, based on the packing volume of the catalyst, was 0.87 s. Blank experiments were performed in the same conditions to evaluate the thermal oxidation.

3.4. Analytical Methods

Post-reaction gases were collected in a Tedlar sampling bag (SKC Inc., Eighty Four, PA, USA) for further analyses. To evaluate the conversion yield, the organic species were determined by means of GC-MS (Agilent 7890A) equipped with a DB 17-MS column (30 m × 0.25 mm, 0.25 μm). [CO] and [CO_2] were measured with an NDIRS on line system (Q-Track Plus IAQ Monitor, TSI), placed at the reactor outlet [23]. [Cl_2] and [HCl] were determined by tritation and ion chromatographic (IC) analyses of two aqueous solutions obtained by bubbling the reactor effluent gases into two water solutions (6 × 10^{-2} M solution of KI and 0.1 M of H_2SO_4 for Cl_2 and 2.6/0.76 mM solution of $NaHCO_3$/Na_2CO_3 for Cl^-). The production of Cl_2 was also assessed by SIM mode GC-MS analysis, using the same operative conditions described for the organic compounds [42]. The reproducibility of the results was checked by triplicate analyses (error < 5%). More details about products characterization are reported in our previous work [19].

The conversion yield was calculated as the ratio between the reacted TCE over the total TCE introduced into the reactor (1):

$$\text{TCE conversion } [\%] \ = \ \frac{m^i_{TCE} - m^o_{TCE}}{m^i_{TCE}} \times 100 \tag{1}$$

where m^i_{TCE} are the moles of TCE introduced into the reactor and m^o_{TCE} are the number of moles measured in the outlet gases; the reaction rate was calculated in terms of converted mass of TCE with respect to the catalyst mass and the residence time of the gas in the reactor (2):

$$\text{conversion rate } \left[\frac{mol}{g \times s} \right] \ = \ \frac{\text{moles of converted TCE}}{\text{catalyst mass } \times \text{ residence time}} \tag{2}$$

4. Conclusions

Iron-doped mayenite catalysts were prepared with different metal loading, obtaining active and selective catalysts able to quantitatively oxidize TCE in the gas phase. All the synthesized catalysts showed good performances for TCE oxidation, totally converted in CO_2, CO, and HCl. Mayenite loaded with 2% iron was found to be the best catalyst in terms of T_{50} (300 °C). This result was correlated with

an optimum combination of the oxidative properties of the mayenite active support with the redox properties of iron, as TPR, XPS, and Raman results have shown.

2.0% Fe/mayenite showed good stability in terms of TCE conversion, respect to pure mayenite. The results only show some deactivation after 12 h of reaction, with a small decrease in the TCE conversion from 95% to 80%. In contrast, pure mayenite had significant deactivation (TCE conversion decrease from 80% to 40%) after 4 h of reaction. The atomic mapping of the samples shows that iron is well dispersed on the mayenite surface, minimizing catalyst deactivation and improving mayenite oxidant activity.

In conclusion, Fe/mayenite was found to be a promising catalyst due to several advantages such as: (i) total conversion of TCE in less-harmful products (CO_2, CO and HCl), (ii) absence of noble and heavy metals, thus reducing costs and the environmental impact, (iii) low cost of catalyst precursors and low deactivation.

Supplementary Materials: The following are available online at http://www.mdpi.com/2073-4344/9/9/747/s1, Figure S1 SEM and EDX analyses of 2.0% Fe/mayenite; Figure S2 XRD patterns of 2.0% Fe/mayenite; Figure S3 SEM and EDX spectrum of 2% Fe/mayenite after reaction; Figure S4 XPS survey spectra of the 2.0% Fe/mayenite.

References

1. Schwille, F. *Dense Chlorinated Solvents in Porous and Fractured Media: Model Experiments*; Lewis Publishers: Boca Raton, FL, USA, 1988; ISBN 978-0-87371-121-0.

2. Russell, H.H.; Matthews, J.E.; Guy, W.S. TCE removal from contaminated soil and ground water. In *EPA Environmental Engineering Sourcebook*; Ann Arbor Press, Inc.: Ann Arbor, MI, USA, 1996.

3. Rossi, F.; Cucciniello, R.; Intiso, A.; Proto, A.; Motta, O.; Marchettini, N. Determination of the trichloroethylene diffusion coefficient in water. *AIChE J.* **2015**, *61*, 3511–3515. [CrossRef]

4. Ko, J.H.; Musson, S.; Townsend, T. Destruction of trichloroethylene during hydration of calcium oxide. *J. Hazard. Mater.* **2010**, *174*, 876–879. [CrossRef]

5. Ge, J.; Huang, S.; Han, I.; Jaffé, P.R. Degradation of tetra- and trichloroethylene under iron reducing conditions by Acidimicrobiaceae sp. A6. *Environ. Pollut.* **2019**, *247*, 248–255. [CrossRef]

6. Moccia, E.; Intiso, A.; Cicatelli, A.; Proto, A.; Guarino, F.; Iannece, P.; Castiglione, S.; Rossi, F. Use of Zea mays L. in phytoremediation of trichloroethylene. *Environ. Sci. Pollut. Res.* **2017**, *24*, 11053–11060. [CrossRef]

7. Meyer, C.; Borgna, A.; Monzon, A.; Garetto, T. Kinetic study of trichloroethylene combustion on exchanged zeolites catalysts. *J. Hazard. Mater.* **2011**, *190*, 903–908. [CrossRef]

8. Cucciniello, R.; Proto, A.; Rossi, F.; Marchettini, N.; Motta, O. An improved method for BTEX extraction from charcoal. *Anal. Methods* **2015**, *7*, 4811–4815. [CrossRef]

9. Intiso, A.; Miele, Y.; Marchettini, N.; Proto, A.; Sánchez-Domínguez, M.; Rossi, F. Enhanced solubility of trichloroethylene (TCE) by a poly-oxyethylene alcohol as green surfactant. *Environ. Technol. Innov.* **2018**, *12*, 72–79. [CrossRef]

10. Garza-Arévalo, J.I.; Intiso, A.; Proto, A.; Rossi, F.; Sanchez-Dominguez, M. Trichloroethylene solubilization using a series of commercial biodegradable ethoxylated fatty alcohol surfactants. *J. Chem. Technol. Biotechnol.* **2019**. [CrossRef]

11. Aranzabal, A.; Ayo, B.P.; González-Marcos, M.P.; González-Marcos, J.A.; López-Fonseca, R.; González-Velasco, J.R. State of the art in catalytic oxidation of chlorinated volatile organic compounds. *Chem. Pap.* **2014**, *68*, 1169–1186. [CrossRef]

12. Li, D.; Li, C.; Suzuki, K. Catalytic oxidation of VOCs over Al- and Fe-pillared montmorillonite. *Appl. Clay Sci.* **2013**, *77*, 56–60. [CrossRef]

13. Tian, W.; Fan, X.; Yang, H.; Zhang, X. Preparation of MnOx/TiO$_2$ composites and their properties for catalytic oxidation of chlorobenzene. *J. Hazard. Mater.* **2010**, *177*, 887–891. [CrossRef]

14. Blanch-Raga, N.; Palomares, A.E.; Martínez-Triguero, J.; Puche, M.; Fetter, G.; Bosch, P. The oxidation of trichloroethylene over different mixed oxides derived from hydrotalcites. *Appl. Catal. B Environ.* **2014**, *160*, 129–134. [CrossRef]

15. Taralunga, M.; Mijoin, J.; Magnoux, P. Catalytic destruction of 1,2-dichlorobenzene over zeolites. *Catal. Commun.* **2006**, *7*, 115–121. [CrossRef]

16. Romero-Sáez, M.; Divakar, D.; Aranzabal, A.; González-Velasco, J.; González-Marcos, J.; Marcos, J.A.G. Catalytic oxidation of trichloroethylene over Fe-ZSM-5: Influence of the preparation method on the iron species and the catalytic behavior. *Appl. Catal. B Environ.* **2016**, *180*, 210–218. [CrossRef]

17. Blanch-Raga, N.; Palomares, A.E.; Triguero, J.M.; Valencia, S. Cu and Co modified beta zeolite catalysts for the trichloroethylene oxidation. *Appl. Catal. B Environ.* **2016**, *187*, 90–97. [CrossRef]

18. Cucciniello, R.; Proto, A.; Rossi, F.; Motta, O. Mayenite based supports for atmospheric NOx sampling. *Atmos. Environ.* **2013**, *79*, 666–671. [CrossRef]

19. Cucciniello, R.; Intiso, A.; Castiglione, S.; Genga, A.; Proto, A.; Rossi, F. Total oxidation of trichloroethylene over mayenite (Ca$_{12}$Al$_{14}$O$_{33}$) catalyst. *Appl. Catal. B Environ.* **2017**, *204*, 167–172. [CrossRef]

20. Intiso, A.; Cucciniello, R.; Castiglione, S.; Proto, A.; Rossi, F. Environmental Application of Extra-Framework Oxygen Anions in the Nano-Cages of Mayenite. In *Advances in Bionanomaterials*; Lecture Notes in Bioengineering; Springer: Cham, Switzerland, 2018; pp. 131–139. ISBN 978-3-319-62026-8.

21. Intiso, A.; Martinez-Triguero, J.; Cucciniello, R.; Proto, A.; Palomares, A.E.; Rossi, F. A Novel Synthetic Route to Prepare High Surface Area Mayenite Catalyst for TCE Oxidation. *Catalysts* **2019**, *9*, 27. [CrossRef]

22. Intiso, A.; Martinez-Triguero, J.; Cucciniello, R.; Rossi, F.; Palomares, A.E. Influence of the synthesis method on the catalytic activity of mayenite for the oxidation of gas-phase trichloroethylene. *Sci. Rep.* **2019**, *9*, 425. [CrossRef]

23. Proto, A.; Cucciniello, R.; Rossi, F.; Motta, O. Stable carbon isotope ratio in atmospheric CO2 collected by new diffusive devices. *Environ. Sci. Pollut. Res.* **2013**, *21*, 3182–3186. [CrossRef]

24. Eufinger, J.-P.; Schmidt, A.; Lerch, M.; Janek, J. Novel anion conductors—Conductivity, thermodynamic stability and hydration of anion-substituted mayenite-type cage compounds C$_{12}$A$_7$:X (X = O, OH, Cl, F, CN, S, N). *Phys. Chem. Chem. Phys.* **2015**, *17*, 6844–6857. [CrossRef]

25. Schmidt, A.; Lerch, M.; Eufinger, J.-P.; Janek, J.; Tranca, I.; Islam, M.M.; Bredow, T.; Dolle, R.; Wiemhofer, H.-D.; Boysen, H.; et al. Chlorine ion mobility in Cl-mayenite (Ca$_{12}$Al$_{14}$O$_{32}$C$_{12}$): An investigation combining high-temperature neutron powder diffraction, impedance spectroscopy and quantum-chemical calculations. *Solid State Ionics* **2014**, *254*, 48–58. [CrossRef]

26. Teusner, M.; De Souza, R.A.; Krause, H.; Ebbinghaus, S.G.; Belghoul, B.; Martin, M. Oxygen Diffusion in Mayenite. *J. Phys. Chem. C* **2015**, *119*, 9721–9727. [CrossRef]

27. Ruszak, M.; Inger, M.; Witkowski, S.; Wilk, M.; Kotarba, A.; Sojka, Z. Selective N$_2$O Removal from the Process Gas of Nitric Acid Plants over Ceramic $_{12}$CaO·$_7$Al$_2$O$_3$ Catalyst. *Catal. Lett.* **2008**, *126*, 72–77. [CrossRef]

28. Proto, A.; Cucciniello, R.; Genga, A.; Capacchione, C. A study on the catalytic hydrogenation of aldehydes using mayenite as active support for palladium. *Catal. Commun.* **2015**, *68*, 41–45. [CrossRef]

29. Ye, T.-N.; Li, J.; Kitano, M.; Hosono, H. Unique nanocages of $_{12}$CaO·$_7$Al$_2$O$_3$ boost heterolytic hydrogen activation and selective hydrogenation of heteroarenes over ruthenium catalyst. *Green Chem.* **2017**, *19*, 749–756. [CrossRef]

30. Li, C.; Hirabayashi, D.; Suzuki, K. A crucial role of O^{2-} and O$_2^{2-}$ on mayenite structure for biomass tar steam reforming over Ni/Ca$_{12}$Al$_{14}$O$_{33}$. *Appl. Catal. B Environ.* **2009**, *88*, 351–360. [CrossRef]

31. Di Carlo, A.; Borello, D.; Sisinni, M.; Savuto, E.; Venturini, P.; Bocci, E.; Kuramoto, K. Reforming of tar contained in a raw fuel gas from biomass gasification using nickel-mayenite catalyst. *Int. J. Hydrog. Energy* **2015**, *40*, 9088–9095. [CrossRef]

32. Mani, S.; Kastner, J.R.; Juneja, A. Catalytic decomposition of toluene using a biomass derived catalyst. *Fuel Process. Technol.* **2013**, *114*, 118–125. [CrossRef]

33. Lacerda, M.; Irvine, J.T.S.; Glasser, F.P.; West, A.R. High oxide ion conductivity in Ca$_{12}$Al$_{14}$O$_{33}$. *Nature* **1988**, *332*, 525–526. [CrossRef]

34. Li, J.; Kitano, M.; Ye, T.-N.; Sasase, M.; Yokoyama, T.; Hosono, H.; Ye, T. Chlorine-Tolerant Ruthenium Catalyst Derived Using the Unique Anion-Exchange Properties of $12CaO \cdot 7Al_2O_3$ for Ammonia Synthesis. *ChemCatChem* **2017**, *9*, 3078–3083. [CrossRef]

35. Diwald, O.; Sterrer, M.; Knözinger, E. Site selective hydroxylation of the MgO surface. *Phys. Chem. Chem. Phys.* **2002**, *4*, 2811–2817. [CrossRef]

36. Ruszak, M.; Witkowski, S.; Sojka, Z. EPR and Raman investigations into anionic redox chemistry of nanoporous $12CaO \cdot 7Al_2O_3$ interacting with O_2, H_2 and N_2O. *Res. Chem. Intermed.* **2007**, *33*, 689–703. [CrossRef]

37. Levasseur, B.; Kaliaguine, S. Effects of iron and cerium in La1−yCeyCo1−xFexO3 perovskites as catalysts for VOC oxidation. *Appl. Catal. B Environ.* **2009**, *88*, 305–314. [CrossRef]

38. Li, H.; Wang, S.; Tang, N.; Pan, S.; Hu, J. FeCl3-modified Co–Ce oxides catalysts for mercury removal from coal-fired flue gas. *Chem. Pap.* **2017**, *71*, 2545–2555. [CrossRef]

39. Grosvenor, A.P.; Kobe, B.A.; Biesinger, M.C.; McIntyre, N.S.; Grosvenor, A. Investigation of multiplet splitting of Fe 2p XPS spectra and bonding in iron compounds. *Surf. Interface Anal.* **2004**, *36*, 1564–1574. [CrossRef]

40. Li, C.; Hirabayashi, D.; Suzuki, K. Synthesis of higher surface area mayenite by hydrothermal method. *Mater. Res. Bull.* **2011**, *46*, 1307–1310. [CrossRef]

41. Molina, R.; Poncelet, G. α-Alumina-Supported Nickel Catalysts Prepared from Nickel Acetylacetonate: A TPR Study. *J. Catal.* **1998**, *173*, 257–267. [CrossRef]

42. Méndez, M.; Ciuraru, R.; Gosselin, S.; Batut, S.; Visez, N.; Petitprez, D. Reactivity of chlorine radical with submicron palmitic acid particles: Kinetic measurements and products identification. *Atmospheric Chem. Phys. Discuss.* **2013**, *13*, 16925–16960. [CrossRef]